Two-phase Flow Modelling for Sediment Transport: Application to Gravity-Driven Flows of Subaqueous Granular Beds

C. Varsakelis[1], D. Monsorno[1] and M.V. Papalexandris[1]

[1] *Institute of Mechanics, Materials, and Civil Engineering,*
Université catholique de Louvain
B-1348, Louvain-la-Neuve, Belgium

Abstract

In the first part of this paper, a two-phase flow model for sediment transport is introduced, based on a mixture theory for fluid–saturated granular materials. This model consists of balance laws of mass and linear momentum for both the sediment and the interstitial fluid and an additional equation for the distribution of particle concentration. The second part of this paper is devoted to numerical aspects of the two-phase flow model in hand and, more specifically, we present a multi-phase projection method, endowed with an interface detection-and-treatment methodology, for its numerical integration. In the final part of this paper, results from numerical studies on gravity–driven flows of erodible, subaqueous granular beds down inclined planes are presented. These results constitute important sanity tests for the assessment of the predictive capacity of the two-phase flow model in hand.

1 Introduction

Sediment transport in coastal areas causes significant morphological changes that can amplify the effects of floods and related inundation hazards. Such unmitigated, and often undesirable, morphological changes increase the risk of failure of near-shore structures. Therefore, they can result in human and animal fatalities, substantial economic losses, and alteration of ecosystems.

Coastal sediment transport is induced by the interaction between turbulence and the solid particles that comprise the sediment. Due to the permeability of the sediment, the interstitial fluid (water) can penetrate it, thus forming a heterogeneous, immiscible mixture. As water flows through and over the sediment, it exerts both normal and shear stresses that engender its erosion.

Modelling of sediment transport is a challenging issue because of the complex interactions between water and sediment, the non-Newtonian behaviour of the latter, and the multitude of spatial and temporal scales that are associated with the flow. Traditionally, in sediment transport studies, the motion of the fluid is modelled either via the shallow water equations [1], or the Boussinesq equation [2], or the Navier-Stokes equations [3]. These equations are then coupled with (semi)empirical formulas for bed sediment transport [4] and an advection/diffusion equation for the suspended sediment [5]. In fact, as regards bed sediment transport, the employment of (semi)empirical formulas extends to both the incipient motion and the sediment flux [6].

Nonetheless, such single-phase flow models and their incarnations, cannot properly account for the interactions between the solid particles and water. To overcome this difficulty, one has to resort to two-phase flow models. The compelling advantage of such models is that they take into consideration the dynamics of both phases and subsume mass and momentum balance laws that are valid both in and over the sediment. Typically, the derivation of two-phase models is based either on an averaging or on a mixture-theory approach. The averaging approach employs aspects from kinetic theories and is based on modifying the equations of motion of a single constituent to account for the presence of the other constituents and then averaging these equations over space and/or time. On the other hand, mixture theories treat the mixture as a multi-component continuum and adopt a non-equilibrium thermodynamic formalism for the derivation of the balance equations for each phase. This is achieved by employing the constraints imposed by the entropy inequality law in order to derive constitutive relations for the irreversible phenomena that take place, such as, viscosity, heat transfer, phase interactions, *etc.*

In this paper, we introduce a two-phase flow model for sediment transport derived from the continuum theory for fluid–saturated granular flows of Papalexandris [7]. This theory constitutes a generalization of the theory of irreversible processes; see, for example, Lebon et al. [8], to open and interacting subsystems with microstructure. The resulting model is valid for both compressible and incompressible flows while simultaneously taking into account the stresses that are developed in the granular medium due to its miscrostructure and the distribution of grains in space. The incompressible limit of this model has been formally derived by Varsakelis and Papalexandris in [9], upon generalization of low-Mach number asymptotics to multi-phase flows.

Following the presentation of the two-phase flow model, we shift our attention to its numerical integration and we delineate an algorithm for two-phase continua, that has been recently proposed by Varsakelis and Papalexandris [10]. This algorithm belongs to the class of projection-type methods, suitably extended to two velocity – two pressure models. One important aspect of this algorithm is its capacity to treat strong material interfaces associated with steep gradients of particle concentration. Finally, we assess the predictive capacity of the model of interest via numerically investigating the evolution of a subaqueous erodible bed in inclined configurations.

2 The Two-Phase Flow Model for Sediment Transport

We consider an isotropic granular material, saturated by a simple fluid, that occupies a domain Ω. Further, we assume that both phases have constant density. Then, according to Varsakelis and Papalexandris [9], the governing equations of the mixture read, in non-dimensional form,

Mass and momentum balance equations for the granular phase,

$$\nabla \cdot \boldsymbol{u}_s = 0\,, \tag{1}$$

$$\begin{aligned}\rho_s\phi_s\frac{\mathrm{d}\boldsymbol{u}_s}{\mathrm{d}_s t} + \nabla(\phi_s p_s) &= \frac{1}{Re}\nabla\cdot(\mu_s\phi_s\,\boldsymbol{V}_s^v)\\ &\quad - \nabla\cdot(\Gamma_s\nabla\phi_s\otimes\nabla\phi_s)\\ &\quad + p_f\nabla\phi_s + \delta\,(\boldsymbol{u}_f-\boldsymbol{u}_s)\\ &\quad + \rho_s\phi_s\boldsymbol{g}\,.\end{aligned} \tag{2}$$

Mass and momentum balance equations for the fluid phase,

$$\nabla\cdot((\boldsymbol{u}_s-\boldsymbol{u}_f)\phi_f) = 0\,, \tag{3}$$

$$\begin{aligned}\rho_f\phi_f\frac{\mathrm{d}\boldsymbol{u}_f}{\mathrm{d}_f t} + \nabla(\phi_f p_f) &= \frac{1}{Re}\nabla\cdot(\mu_f\phi_f\,\boldsymbol{V}_f^v)\\ &\quad - (p_f\nabla\phi_s + \delta\,(\boldsymbol{u}_f-\boldsymbol{u}_s))\\ &\quad + \rho_f\phi_f\boldsymbol{g}\,.\end{aligned} \tag{4}$$

Compaction equation,

$$\frac{\mathrm{d}\phi_s}{\mathrm{d}_s t} = 0\,. \tag{5}$$

Here, the subscripts "s" and "f" denote the granular and fluid phase, respectively. Further, ρ_i, ϕ_i and $\boldsymbol{u}_i = (u_{i_1}, u_{i_2}, u_{i_3})$, $i = s, f$ are the density, volume fraction and velocity vector of the phase i. Also, p_s and p_f are the "dynamic" pressures of the granular and fluid phase, respectively; they are completely equivalent to the pressure term that appears in the Navier-Stokes equations. Additionally, μ_i is the viscosity coefficient of the phase i and $\mathbf{g}$ is the gravity vector. We note that μ_s, which describes the rheology of the granular material, is not constant but depends, among others, on the particle concentration.

The operators $\frac{\mathrm{d}}{\mathrm{d}_i t} = \frac{\partial}{\partial t} + \mathbf{u}_i\cdot\nabla$ and $\mathbf{V}_i^v$ stand for the material derivative and the traceless deviatoric part of the deformation tensor of phase i, $i = s, f$, respectively. The above governing equations are closed by the saturation condition,

$$\phi_s + \phi_f = 1\,. \tag{6}$$

The momentum exchange between the two phases is represented by the combined term $p_f\nabla\phi_s + \delta(\boldsymbol{u}_f - \boldsymbol{u}_s)$, appearing in the right-hand side of the momentum equations 2 and 4, albeit with opposite sign. More specifically, the term $\delta(\boldsymbol{u}_f - \boldsymbol{u}_s)$ models the interphasial drag exerted on the solid particles by the fluid, with δ being the interphasial drag coefficient. Further, the non-conservative product $p_f\nabla\phi_s$ models nozzling effects and its presence is dictated by thermodynamic considerations.

The term $\Gamma_s\nabla\phi_s\otimes\nabla\phi_s$, whose divergence enters the momentum equation of the granular phase, 2, is the so-called *configuration stress tensor* and, accordingly, Γ_s is the *configuration stress coefficient*. This tensor represents stresses developed from rearrangements in the distribution of the interfacial area density. Moreover, it constitutes the non-dissipative part of the Cauchy stress tensor of the granular material. At equilibrium, its off-diagonal components model shear stresses that such materials support due to their micro-structure.

2.1 A Numerical Method for the Two-Phase Flow Model

Varsakelis and Papalexandris [10] proposed an algorithm for the integration of equations 1–5; see also the more recent article of Varsakelis et al. [11]. This algorithm constitutes a generalization of projection-type methods on collocated grids to two-phase flow models and employs a predictor–corrector scheme the integration in time. Due to the presence of two momentum equations, a double projection is employed; one for each velocity vector. Accordingly, a Poisson equation and a second-order elliptic PDE with variable coefficient are solved at both the prediction and the correction stages for the computation of the pressures of the granular and fluid phase, respectively. The generalized flux–interpolation method proposed in Lessani and Papalexandris [12] is employed for the integration of the convective terms to remedy the well-known odd–even decoupling phenomenon. Additionally, stiffness problems due to steep volume–fraction gradients in the vicinity of material interfaces are treated via a regularization method. Schematically, the flowchart of the algorithm reads:

i) The values of the volume fraction, ϕ_s are computed by integrating the compaction equation 5 via the multi-dimensional upwind scheme of Colella [13].

ii) The algorithm searches for interfaces by checking the magnitude of $\nabla\phi_s$. In the vicinity of the interface, the predicted values of ϕ_s are replaced by those of smoother, compactly supported function obtained through a parabolic regularization.

iii) A projection method is employed for the computation of the the granular pressure p_s and velocity $\mathbf{u}_s$. In particular, the pressure p_s is computed via solving numerically a Poisson equation. Once p_s has been computed, $\mathbf{u}_s$ is calculated via the standard Helmholtz decomposition.

iv) In our case, $\mathbf{u}_f$ is not divergence free; see equation 3, which requires a generalization of the standard projection method. This results in a second order elliptic PDE with variable coefficients for the pressure p_f. Once p_f is computed, then $\mathbf{u}_f$ is calculated via the Helmholtz-Marsden decomposition.

3 Numerical Results

In this section, the two-phase flow model at hand is employed to investigate the motion of an subaqueous erodible granular bed down an inclined plane. The objective of this numerical study is twofold. First, to systematically study the properties of the flows of interest and gain physical insight on the mechanisms that drive their evolution. In this respect, emphasis is placed on the deformation of the material interface between the granular bed and the interstitial fluid lying above it. Second, to assess the predictive capacity of the model in hand for the flows of interest.

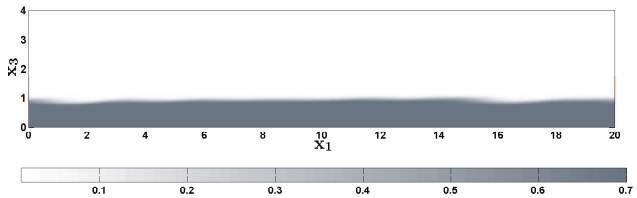

(a)

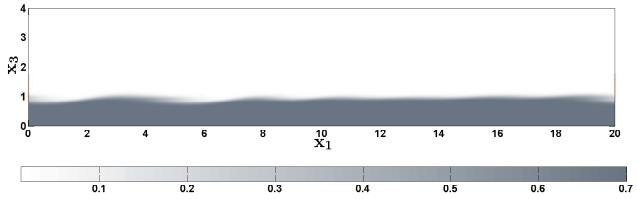

(b)

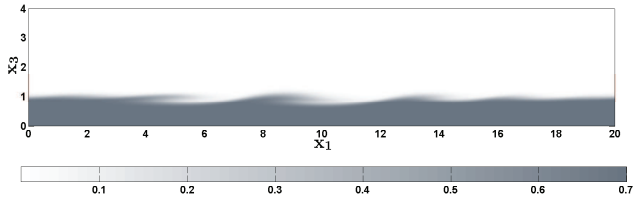

(c)

For clarity purposes, all dimensional variables are denoted with a hat symbol, "ˆ".

3.1 Mixture Parameters and Computational Set-up

We consider a mixture of water with coarse sand. The sand is assumed to be monodisperse and its diameter $\hat{d}_p$ is taken equal to $1\,mm$. The densities of water and sand are $\hat{\rho}_f = 1000\ kg/m^3$ and $\hat{\rho}_s = 2200\ kg/m^3$, respectively.

As regards the configuration stress coefficient Γ_s, we assume the following expression,

$$\hat{\Gamma}_s \;=\; \hat{k}_2 \hat{\rho}_s \phi_s \,. \tag{7}$$

Here, $\hat{k}_2$ is a (strictly positive) material-dependent constant and its value should be obtained experimentally. However, systematic experimental measurements for $\hat{k}_2$ have yet to appear in the literature. On the other hand, Varsakelis and Papalexandris [14] estimated numerically the value of $\hat{k}_2$ by computing the equilibrium distributions of granular materials and the forces acting on them. On the basis of this study, we choose $\hat{k}_2 = 4 \times 10^{-5}\ m^4/s^2$.

For the rheology of the granular material we opt for the experimental correlation derived by Savage [15],

$$\hat{\mu}_s \;=\; \frac{\hat{\mu}'_s \phi_s}{(\phi_c - \phi_s)^2} \,, \tag{8}$$

where the parameter ϕ_c represents the maximum packing of grains. Following Passman et al. [16], the value of $\hat{\mu}'_s$ is set equal to 723 $kg/(m \cdot s)$. The blow-up of 8 at $\phi_s = \phi_c$ is intended to represent the "jamming" effect that grains experience upon attaining their maximum packing. However, the effects of this singularity have not been explored, either theoretically or numerically. For this reason, we have assumed that $\phi_c = 1$, so that μ_s remains bounded. On the other hand, the interstitial fluid, water, is assumed to be a simple Newtonian fluid at constant temperature. As such, its viscosity is taken to be constant and equal to $\hat{\mu}_f = 1 \times 10^{-3}\ kg/(m \cdot s)$.

As regards the interphasial drag coefficient $\hat{\delta}$, the force density exerted by the fluid on the particles is approximated by the drag on a sphere moving at constant speed at low Reynolds numbers. This results in the following expression for $\hat{\delta}$,

$$\hat{\delta} \;=\; \phi_s \, 18 \, \frac{\hat{\mu}_f}{\hat{d}_p^2} \, Q(Re_p) \,. \tag{9}$$

For the function $Q(Re_p)$, the empirical relationship proposed by Rowe [17] is used,

$$Q(Re_p) \;=\; \begin{cases} 1 + 0.15\ Re_p^{0.687}, & Re_p < 1000 \,, \\ 0.01833\ Re_p, & Re_p \geq 1000 \,, \end{cases} \tag{10}$$

where Re_p is the particle Reynolds number, defined with respect to the relative grain velocity, *i.e.*,

$$Re_p \;=\; \frac{\hat{\rho}_f \, \hat{d}_p}{\hat{\mu}_f} |\hat{\boldsymbol{u}}_s - \hat{\boldsymbol{u}}_f| \,. \tag{11}$$

In our study, all physical parameters are non-dimensionalized as follows. The phasial densities and pressures have been non-dimensionalized with respect to the density of water, $\hat{\rho}_{ref} = 1000\ kg/m^3$, and atmospheric pressure, $p_{ref} = 10^5\ Pa$, respectively. Also, the initial thickness of the granular layer, $\hat{h}$, and the reference velocity $u_{ref} = \sqrt{\hat{g}\,\hat{h}}$ have been used for the non-dimensionalization of lengths and velocities, respectively. Further, the viscosity coefficients have been non-dimensionalized with respect to the mixture's viscosity $\mu_{ref} = (\rho_s \phi_{s,in} \mu_s + \rho_f \phi_{f,in} \mu_f)/(\rho_s \phi_{s,in} + \rho_f \phi_{f,in})$, where $\phi_{s,in}$ stands for the initial distribution of particles. For the problem in hand, $\mu_{ref} \equiv 608\ kg/(m \cdot s)$ and, accordingly, the Reynolds number of the flow is equal to approximately 0.2.

3.2 Subaqueous Granular Bed Inclined at 30^o.

The unsteady, gravity-driven flow of a subaqueous erodible granular bed on a plane inclined at 30^o, with the above mixture parameters, has been studied via direct numerical simulations in Varsakelis and Papalexandris [18]. Herein, we confine ourselves to a brief presentation of the the main findings and refer the reader to [18] for additional information. For the sake of completeness, we also discuss the computational set-up of the numerical experiments.

The mixture is placed on the surface of a plane inclined at an angle 30^o to the streamwise direction. A Cartesian coordinate system is employed with x_1 the streamwise and x_3 the normal direction. The dimensions of the computational domain are $l = 20$ and 4 in the streamwise and normal directions, respectively and an equidistant mesh of 500×100 cells is used for its discretization. Finally, we set $\Delta t = 0.005\ \Delta x_3$.

As regards boundary conditions, the flow is assumed to be periodic in the streamwise (x_1) direction, with period

equal to l. At the bottom of the computational domain, which coincides with the inclined plane, the no-slip condition is prescribed for the phasial velocities and zero-Neumann conditions are prescribed for both the phasial pressures and the volume fraction. On the other hand, the top boundary of the computational domain is considerably far from the material interface. For this reason, at this boundary, the free-slip boundary condition is applied for the phasial velocities whereas zero-Neumann conditions are assigned to the phasial pressures and the volume fraction.

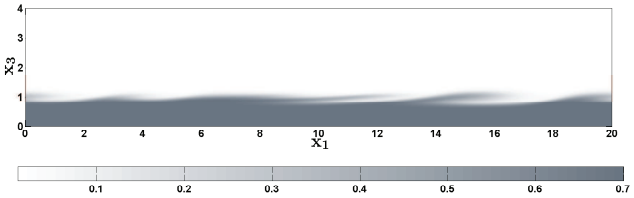

(d)

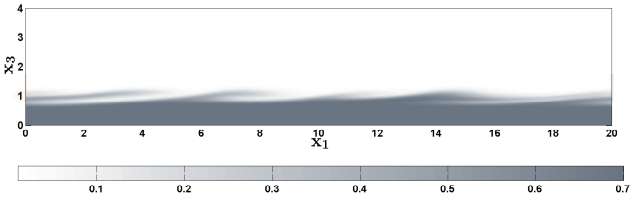

(e)

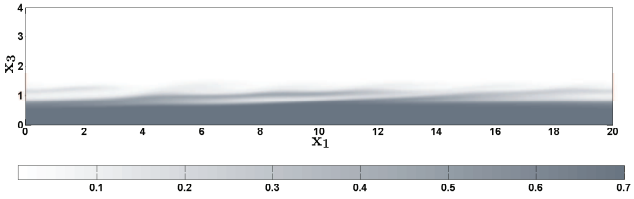

(f)

Figure 1: Iso-contours of particle concentration ϕ_s. (a) $t = 24.5$, (b) $t = 30$, (c) $t = 37$, (d) $t = 43$, (e) $t = 49$, (f) $t = 73$. The material interface deforms into a series of long waves due to the onset of the Kapitza instability. The Kapitza waves are transformed into skewed, vortex ripples that grow in time and also coalesce. Eventually, the fluid velocity becomes large enough in the neighbourhood of the interface and the ripples are washed out

For the initial condition of the particle concentration, we consider a dense ($\phi_s = 0.7$) granular layer of constant thickness $h = 1$, placed on the inclined plane. This profile is superimposed to a sinusoidal perturbation of period l and amplitude $h/5$, so as to trigger the erosion of the material interface. Outside the granular bed, the domain is filled with water. As regards the initial conditions for the other variables, we assume that the entire mixture is at rest so that the flow is induced by gravity.

Figures 1(a)–1(f) show the particle concentration at various time instances. Our simulations show that the evolution of the flow can be divided into three distinct phases. The first phase, which lasts until approximately $t \simeq 36.7$, is characterized by the onset of the Kapitza instability and the deformation of the material interface into a series of long waves. In the second phase, which starts at $t \simeq 36.7$ and lasts until $t \simeq 62$, the Kapitza waves transform into skewed vortex ripples. As the flow evolves, the ripples grow and eventually coalesce. In the third phase, which spans from $t \simeq 61.2$ until the termination of the simulation, the high fluid velocities wash out these ripples and a layer of rapidly moving particles forms at the material interface.

Let $\overline{u}_{s_1}$ denote the normalized, streamwise–averaged, granular velocity component, in the streamwise direction. 2 shows plots of $\overline{u}_{s_1}$, against depth x_3, at different time instances. The velocities are maximized at the material interface. Away from it they decrease to zero, however, no rigid body motion is observed, even close to the inclined plane. This result is in very good agreement with the analysis of Andreotti and Douady [19], which asserts that, for angles of inclination $a \geq 25^o$, the flowing height reaches the inclined plane.

2 additionally yields that the predicted velocity profiles collapse very well to a master linear curve that has small negative curvature at the vicinity of the material interface; this is evidence that the flow evolves in a self–similar manner. According to previous experimental and numerical studies on dry granular flows with large angles of inclination, the profiles of $\overline{u}_{s_1}$ are approximately linear, with positive curvature at the upper part and negative curvature at the lower part; see, for example, Andreotti and Douady [19]. Further, these studies show that for $a \geq 30^o$, the profiles become predominantly linear. Self-similar behaviour has also been reported in the experiments of dry granular avalanches of Bonamy et al. [20]. Our simulations provide the first evidence that these properties extend over to unsteady flows of fluid-saturated granular materials as well. Finally, it is worth noting that the aforementioned similarity between the $\overline{u}_{s_1}$ profiles in dry and fluid-saturated granular flows has already been confirmed experimentally for steady flows; see Jain et al. [21], Doppler et el. [22] and others.

The examination of the vorticity field of the fluid provides important information about the nature of the observed ripples. Figures 3(a)–3(c) depict iso-contours of the magnitude of the fluid phase vorticity field at times $t = 30$, 43 and 73, respectively. The shearing of the granular medium by the interstitial fluid engenders vortex shedding from the material interface. These vortices are skewed, with their streamwise-diameter being nearly ten times large than the normal one, and undergo streamiwise elongation as the flow evolves. Moreover, since the observed vortices are located downstream each ripple's crest,in accordance with Bagnold's classical terminology, the ripples are actually *vortex* ripples.

4 Conclusions

In the present article, a two-phase model for sediment transport has been presented. This model is derived from a particular mixture theory for fluid–saturated granular materials and comprises balance laws for both the fluid and the granular phase plus an additional equation that governs the evolution of the volume fraction. Further, it properly accounts for the momentum exchanges between the two phases in a thermodynamically consistent manner. Also, the model of interest allows for non-zero shear stresses at zero shear rates, which constitutes an important characteristic of granular materials.

Following the exposition of the two-phase flow model, an algorithm for its numerical treatment has been presented. This is a predictor–corrector numerical method that employs a double projection for the computation

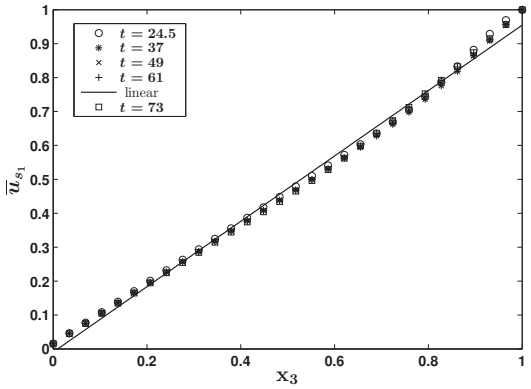

Figure 2: Granular velocity profiles $\overline{u}_{s_1}$ plotted against depth at various times. The predicted velocities collapse onto a master linear curve, with a slightly negative curvature close to the material interface. This collapse indicates that the flow evolves in a self-similar manner

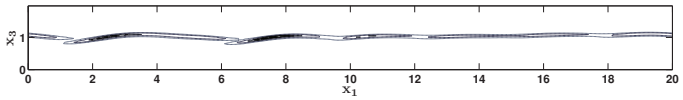

(a)

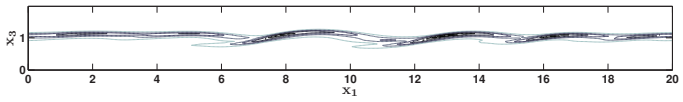

(b)

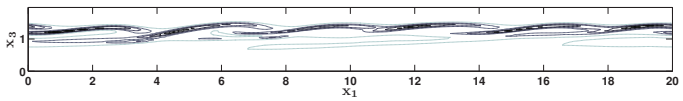

(c)

Figure 3: Iso-contours of the vorticity field of the fluid phase at (a) $t = 30.6$, (b) $t = 43$, (c) $t = 73$. Vortical structures are observed over the material interface. At $t = 43$, when the ripples have been formed, lee vortices are formed downstream the crest of each ripple

of the phasial velocities and pressures; one for each velocity vector. For the numerical treatment of material interfaces, the algorithm is combined with an interface detection-and-treatment methodology which is based on a local regularization scheme.

The predictive capacity of the two-phase flow model of interest, has been assessed via direct numerical simulations of a gravity–driven flow of an erodible, subaqueous granular bed down an inclined plane. Overall, the numerical predictions adduce that the two-phase flow model at hand can reproduce the important characteristics of the flows of interest.

Acknowledgment

Financial support for the first author has been provided by the National Research Fund of Belgium (FNRS) under the GRANMIX Projet de Recherche. The second and third authors gratefully acknowledge the financial support of the European Union via SEDITRANS, a project funded by the Marie Curie Actions of the EU's 7th Framework Programme.

References

[1] M. J. Diaz, E. D. Fernandez–Nieto, and A. M. Ferreiro, "Sediment transport models in shallow water equations and numerical approach by high order finite volume methods," *Comp. Fluids*, vol. 37, pp. 299–316, 2008.

[2] H. A. Shäffer, P. A. Madsen, and R. Deigaard, "A boussinesq model for waves breaking in shallow water," *Coast. Eng.*, vol. 20, pp. 185–202, 1993.

[3] A. S. Dimakopoulos and A. A. Dimas, "Large-wave simulation of three-dimensional, cross-shore and oblique, spilling breaking on constant slope beach," *Coast. Eng.*, vol. 58, pp. 790–801, 2011.

[4] P. T. Nam, M. Larson, H. Hanson, and L. X. Hoan, "A turbulent and suspended sediment transport model for plunging breakers," *Coast. Eng.*, vol. 56, pp. 1084–1096, 2009.

[5] B. Ontowirjo and A. Mano, "A turbulent and suspended sediment transport model for plunging breakers," *Coast. Eng. J.*, vol. 50, pp. 349–367, 2008.

[6] B. Camenen and P. Larroude, "Comparison of sediment transport formulae for the coastal environment," *Coast. Eng.*, vol. 48, pp. 111–132, 2003.

[7] M. V. Papalexandris, "A two-phase model for compressible granular flows based on the theory of irreversible processes," *J. Fluid Mech.*, vol. 517, pp. 103–112, 2004.

[8] D. G. Lebon, D. Jou, and J. Casas-Vázquez, *Understanding Non-equilibrium Thermodynamics: Foundations, Applications, Frontiers*. Springer, 2008.

[9] C. Varsakelis and M. V. Papalexandris, "Low-mach-number asymptotics for two-phase flows of granular materials," *J. Fluid Mech.*, vol. 669, pp. 472–497, 2011.

[10] C. Varsakelis and M. V. Papalexandris, "A numerical method for two-phase flows of dense granular mixtures," *J. Comput. Phys.*, vol. 257, pp. 737–756, 2014.

[11] C. Varsakelis, D. Monsorno, and M. V. Papalexandris, "Numerical aspects of two pressure – two velocity models." submitted for publication, 2014.

[12] B. Lessani and M. V. Papalexandris, "Time-accurate calculation of variable density flows with strong temperature gradients and combustion," *J. Comput. Phys.*, vol. 212, pp. 218–246, 2006.

[13] P. Colella, "Multidimensional upwind methods for hyperbolic conservation laws," *J. Comput. Phys.*, vol. 87, pp. 171–200, 1990.

[14] C. Varsakelis and M. V. Papalexandris, "The equilibrium limit of a constitutive model for two-phase granular mixtures and its numerical approximation," *J. Comput. Phys.*, vol. 229, pp. 4183–4207, 2010.

[15] S. B. Savage, "Gravity flow of cohesionless granular materials in chutes and channels," *J. Fluid Mech.*, vol. 92, pp. 53–96, 1979.

[16] S. L. Passman, J. W. Nunziato, and P. B. Bailey, "Shearing motion of a fluid-saturated granular material," *J. Rheol.*, vol. 20, pp. 167–192, 1986.

[17] P. N. Rowe, "Drag forces in a hydraulic model of a fluidised bed. part ii," *Trans. Int. Chem. Engng*, vol. 48, pp. 175–180, 1961.

[18] C. Varsakelis and M. V. Papalexandris, "Numerical simulation of unsteady chute flows of fluid-saturated granular materials." submitted for publication, 2014.

[19] B. Andreotti and S. Douady, "Selection of velocity profile and flow depth in granular flows," *Phys. Rev. E*, vol. 63, p. 031305, 2001.

[20] D. Bonamy, F. Daviaud, and L. Laurent, "Experimental study of granular flows via a fast camera: a continuous description," *Phys. Fluids*, vol. 14, pp. 1666–1673, 2002.

[21] N. Jain, J. M. Ottino, and R. M. Lueptow, "Effect of interstitial fluid on a granular flow layer," *J. Fluid Mech.*, vol. 508, pp. 23–44, 2004.

[22] D. Doppler, P. Gondret, T. Loiseleux, S. Meyer, and M. Rabaud, "Relaxation dynamics of water–immersed granular avalanches," *J. Fluid Mech.*, vol. 577, pp. 161–181, 2007.